Langmuir

ARTICLE

pubs.acs.org/Langmuir

A Model of Electrowetting, Reversed Electrowetting, and Contact Angle Saturation

Dan Klarman and David Andelman*

Raymond & Beverly Sackler School of Physics and Astronomy, Tel-Aviv University, Ramat Aviv 69978, Tel Aviv, Israel

Michael Urbakh

Raymond & Beverly Sackler School of Chemistry, Tel-Aviv University, Ramat Aviv 69978, Tel Aviv, Israel

ABSTRACT: While electrowetting has many applications, it is limited at large voltages by contact angle saturation, a phenomenon that is still not well understood. We propose a generalized approach for electrowetting that, among other results, can shed new light on contact angle saturation. The model assumes the existence of a minimum (with respect to the contact angle) in the electric energy and accounts for a quadratic voltage dependence $\sim U^2$ in the low-voltage limit, compatible with the Young−Lippmann formula, and an $\sim U^{-2}$ saturation at the high-voltage limit. Another prediction is the surprising possibility of a reversed electrowetting regime, in which the contact angle increases with applied voltage. By explicitly taking into account the effect of the counter-electrode, our model is shown to be applicable to several AC and DC experimental electrowetting-on-dielectric (EWOD) setups. Several features seen in experiments compare favorably with our results. Furthermore, the AC frequency dependence of EWOD agrees quantitatively with our predictions. Our numerical results are complemented with simple analytical expressions for the saturation angle in two practical limits.

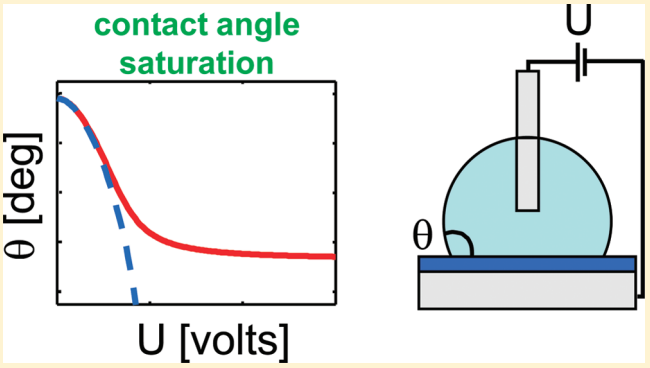

I. INTRODUCTION

The term electrowetting, in its broadest sense, refers to techniques by which one can control the apparent wettability (characterized by the contact angle) of liquids, by applying an external electric potential.[1−11] While it has numerous applications,[12−20] electrowetting is known to be limited by the so-called contact angle saturation (CAS)[5,7,21−27] as depicted in Figure 1. As the term indicates, an electric potential can incur a change in the contact angle, but only to a certain extent. Further voltage increase has no additional effect on the contact angle. This behavior is not accounted for by the standard model of electrowetting, and its origin still remains a point of controversy.[5−7,12,21−33]

When a small drop of liquid is placed on top of a solid surface, it assumes the shape of a spherical cap.[34] The contact angle θ_0 between the drop and the surface, given by the Young formula,[34−36]

$$\cos\theta_0 = \frac{\gamma_{sa} - \gamma_{sl}}{\gamma_{la}} \qquad (1)$$

depends on the three interfacial tensions: solid/air γ_{sa}, solid/liquid γ_{sl}, and liquid/air γ_{la}, where the air phase can be replaced by another immiscible fluid.[7,17,19]

The Young formula, eq 1, can be obtained by minimizing the capillary free energy with a fixed volume constraint[36]

$$F_{cap}(\theta) = A_{sa}\gamma_{sa} + A_{sl}\gamma_{sl} + A_{la}\gamma_{la} - V\Delta P \qquad (2)$$

where A_{ij} are the interface areas between the i and j phases, i,j = a (air), l (liquid), and s (solid); the drop volume is V, and the pressure difference across the liquid/air interface is ΔP. For partial wetting, $\gamma_{sa} < \gamma_{sl} + \gamma_{la}$, the capillary free energy F_{cap} has a minimum at the Young angle, θ_0 (Figure 2a).

The contact angle θ can be varied from its initial value θ_0 by applying an external voltage of several volts to several hundreds of volts across the liquid drop. A commonly used electrowetting setup developed by Rinkel et al.[1] and later perfected by Vallet et al.[5] is called electrowetting-on-dielectric (EWOD). The apparatus, roughly sketched in Figure 3a, includes a flat electrode as a substrate, which is coated with a thin dielectric layer (tens of nanometers to several micrometers thick), whose purpose is to prevent Faradic charge exchange (i.e., electrochemical reactions) at the electrode. It is common that this dielectric layer is then topped with an even thinner hydrophobic (i.e., Teflon) layer in order to control its surface tension. A drop of ionic solution is placed atop the coated electrode, and a thin counter-electrode (usually a bare platinum fiber) is inserted into the drop from above. The drop is surrounded by air or by another

Received: February 1, 2011
Revised: March 23, 2011
Published: April 21, 2011

ACS Publications © 2011 American Chemical Society

dx.doi.org/10.1021/la2004326 | *Langmuir* 2011, 27, 6031–6041

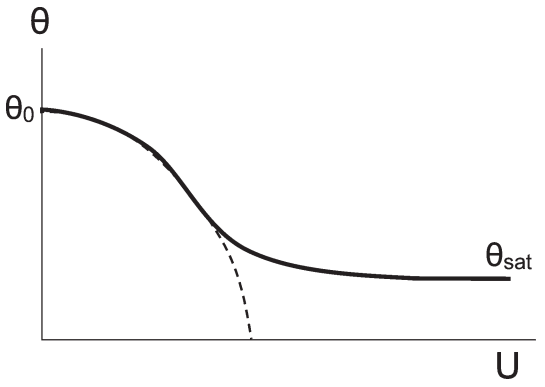

Figure 1. Schematic plot of electrowetting contact angle, $\theta(U)$. For zero voltage, the contact angle is the same as the Young angle, θ_0. At low applied voltages, U, the contact angle follows the Young−Lippmann formula, eq 6 (dashed line), $\cos\theta(U) - \cos\theta_0 \simeq \cos\theta_{YL}(U) - \cos\theta_0 \sim U^2$, but for higher voltages the contact angle gradually deviates from the Young−Lippmann behavior and saturates toward some finite value, θ_{sat}.

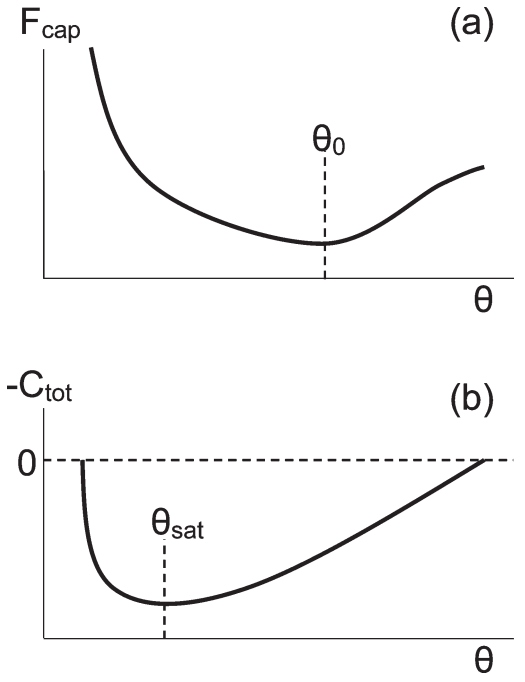

Figure 2. Schematic plots of (a) the capillary free energy F_{cap} for a spherical drop of fixed volume and (b) a hypothetical (negative) total capacitance, $-C_{tot}$, as function of contact angle θ in the electrowetting setup. The minimum of the capillary term F_{cap} occurs at the Young angle θ_0, while the electric term $F_{el} = -{}^1/_2 C_{tot} U^2$ (or equivalently of $-C_{tot}$) is assumed to have a minimum at a finite saturation angle, θ_{sat}.

immiscible dielectric liquid. Applying a voltage across the drop can cause a large change, of several tens of degrees, in the contact angle.

As reviewed in ref 12, a simple relation between the contact angle and the applied voltage can be derived. When an external voltage U is applied, an electric double layer is formed at the liquid/substrate interface. The total free energy F_{tot} has two contributions: a capillary term F_{cap} defined[37] in eq 2, and an

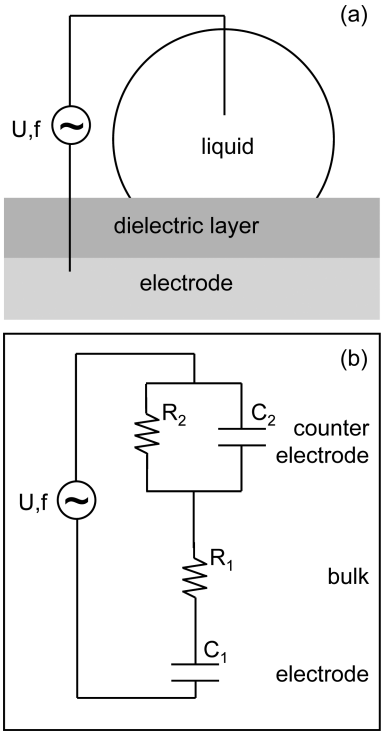

Figure 3. (a) Sketch of an EWOD setup with AC voltage U of frequency f and (b) its equivalent AC circuit. The two parallel-plate capacitors of capacitances C_1 and C_2 and areas A_1 and A_2 represent the substrate/liquid and the counter-electrode/liquid interfaces, respectively. The bulk liquid drop is represented by a resistor R_1 through which the two capacitors are charged and discharged. The charging time through the resistor is equal to the build-up time τ_b of the double layers at the two interfaces. The discharge resistor R_2 represents the Faradic charge transfer processes that relax the electric double layer near the counter-electrode with relaxation time τ_r. Such a mechanism is prevented at the substrate electrode because of its dielectric coating.

electric term F_{el} that depends on θ, U, and other system parameters.

$$F_{tot}(\theta, U) = F_{cap}(\theta) + F_{el}(\theta, U) \tag{3}$$

Within the standard model of electrowetting (under external voltage control), the electric term is evaluated as

$$F_{el} = -\frac{1}{2} C_{ld} U^2 \tag{4}$$

where C_{ld} is the capacitance of the liquid/substrate interface, which is modeled as a parallel-plate capacitor:

$$C_{ld} \simeq \varepsilon_0 A_{ld} \left(\frac{d}{\varepsilon_d} + \frac{\lambda_D}{\varepsilon_l} \right)^{-1} \simeq \frac{\varepsilon_0 \varepsilon_d}{d} A_{ld} \tag{5}$$

where A_{ld} is the substrate area that is covered by the liquid drop, d is the width of the dielectric layer, and ε_d and ε_l are the dielectric constants of the dielectric coating and liquid drop, respectively. The Debye screening length, λ_D, is the width of the electric double layer. In most cases, $d/\varepsilon_d \gg \lambda_D/\varepsilon_l$, and the second approximation in eq 5 can be justified. The parallel-plate capacitor model has been shown[10] to be valid as long as fringe fields are negligible ($d \ll A_{ld}{}^{1/2}$) and the drop of volume V is not too small for double layers to be created ($\lambda_D \ll V^{1/3}$). An implicit

dx.doi.org/10.1021/la2004326 |Langmuir 2011, 27, 6031–6041

assumption made in eq 4 is that the counter-electrode does not contribute to the total capacitance.

In an electrowetting setup, the contact angle $\theta(U)$ depends on the external voltage U. By substituting eq 5 into eq 4 and minimizing F_{tot} of eq 3 with a fixed volume constraint, the Young–Lippmann formula[12] for the contact angle $\theta_{YL}(U)$ is obtained

$$\cos\theta_{YL}(U) = \cos\theta_0 + g^{-1}U^2 \quad (6)$$

where $g^{-1} \equiv \varepsilon_0\varepsilon_d/(2\gamma_{la}d)$. It is a common practice to extend this DC voltage model to AC setups by using the root mean square (rms) voltage in eq 6, $U^2 \rightarrow U_{rms}^2$. Note that similar results can be obtained using force balance at the three-phase contact line.[38]

Experiments[5−7,12,21−24,29−31] have shown that the $\sim U^2$ behavior predicted by the Young–Lippmann formula is indeed found for a range of low applied voltages, but the prefactor of the U^2 term, eq 6, does *not* usually match the experimental data. For larger values of U, a deviation from the U^2 behavior is observed and a saturation in the contact angle, $\theta(U) \rightarrow \theta_{sat}$, is reached gradually, as is schematically sketched in Figure 1. In addition, it is convenient to define a characteristic value of the crossover voltage U^* by requiring that $\theta_{YL}(U^*) = \theta_{sat}$ in eq 6:

$$(U^*)^2 = g(\cos\theta_{sat} - \cos\theta_0) \quad (7)$$

Over the last decades, several models have been presented in an attempt to explain CAS.[12] Most of these models[7,22,26,31−33] are based on specific leakage mechanisms. Others, as in ref 24, proposed heuristic arguments in order to predict CAS in electrowetting systems without relying on a specific mechanism.

Considering that the origin of CAS is not well understood from general principles, the objective of the present work is to offer a different approach to CAS, and to electrowetting in general. In the following section, we consider the general circumstances in which CAS can occur intrinsically (without leakage). We present a low-voltage limit compatible with the Young–Lippmann quadratic voltage dependence and a high-voltage limit in which CAS is obtained. Furthermore, we identify a possibility for a novel electrowetting regime we call *reversed electrowetting*. In section III, we present an application of this approach to EWOD experimental setups using a geometry-dependent model, and use AC circuit analysis to calculate the free energy. Section IV is dedicated to showing several numerical and analytical results and their compatibility with experiments. We conclude in section V with a summary along with some further discussion and an outlook on future research.

II. A GENERALIZED MODEL OF ELECTROWETTING

A. Generalized Free Energy and Contact Angle Saturation. Our starting point is eq 3 above. Assuming that all the electric energy is stored via charge separation, it can be written in terms of the total capacitance, $F_{el} = -{}^1/_2 C_{tot}U^2$. The total *electrocapillary* free energy F_{tot} is now written as

$$F_{tot}(\theta, U) = F_{cap}(\theta) - \frac{1}{2}C_{tot}(\theta)U^2 \quad (8)$$

where all capillary contributions are included in F_{cap}. As F_{cap} is independent of U, the relative magnitude of the two terms in eq 8 is controlled by the negative U^2 dependence of the F_{el} term.

Physical insight can be gained from eq 8 by making different assumptions regarding the behavior of $C_{tot}(\theta)$. Particularly, interesting results follow from the assumption that $C_{tot}(\theta)$ has a maximum at some finite angle (see Figure 2b), as will be shown below to be the case for EWOD setups. Our model therefore differs from previous models that took C_{tot} to be equal to C_{ld} (eq 4), which yields a monotonically decreasing F_{el}. For reasons to be immediately apparent, we denote the angle where $C_{tot}(\theta)$ has a maximum (or, equivalently, F_{el} has a minimum) as θ_{sat}. This angle, in general, is different from the Young angle, θ_0, which minimizes the capillary term, F_{cap}.

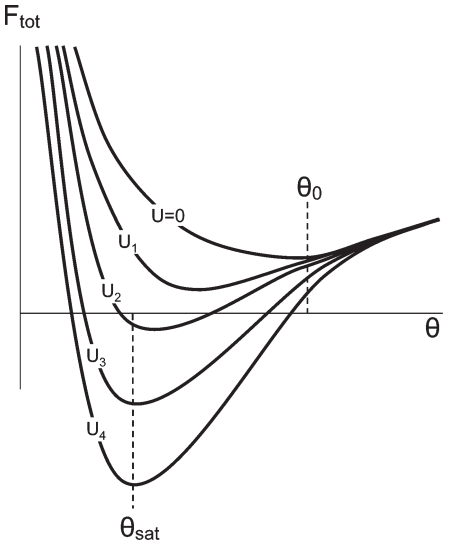

Figure 4. Schematic plot of the total free energy $F_{tot}(\theta,U) = F_{cap}(\theta) + F_{el}(\theta,U)$ for a sequence of five applied voltages: $U_4 > U_3 > U_2 > U_1 > U = 0$. Since the two energy terms are concave in the accessible range of θ, their sum is also concave and has a minimum. Increasing U from zero to a large U_4 causes a gradual shift of the minimum from θ_0 toward θ_{sat}. Note that it cannot cross beyond θ_{sat} regardless of how high the voltage U is because θ_{sat} is the minimum of the dominating F_{el} term.

We now show how the existence of a global electric free-energy minimum at a finite contact angle yields CAS. With no applied voltage ($U = 0$), $F_{tot} = F_{cap}$ and the system adheres to the Young angle, $\theta = \theta_0$ (Figure 2a). Similarly, when the applied voltage U is very large, the free energy is dominated by the electric term, $|F_{el}| \propto U^2 \gg F_{cap}$, and the system tends toward θ_{sat}, which minimizes F_{el} (or, equivalently, maximizes C_{tot}; Figure 2b). Now, if the two contributions are concave for the accessible range of θ, then the minimum of F_{tot} shifts smoothly from θ_0 toward θ_{sat} as U is increased from zero to an arbitrary large value, as is schematically illustrated in Figure 4. This description is consistent with CAS and implies that the saturation angle found in experiments can be identified with our definition of θ_{sat}.

Below we analyze more quantitatively the consequences of such a global electric minimum at the low- and high-voltage limits. In the former, we show an $\sim U^2$ variation of the contact angle with a prefactor that can match the Young–Lippmann formula or be different from it. In the latter, an asymptotic $\sim U^{-2}$ approach to θ_{sat} is found.

B. The Low Voltage Limit. For $U \rightarrow 0$, the minimum of F_{tot} occurs close to θ_0. Expanding this minimum condition $F'_{tot}(\theta) = 0$ to first order in $\delta\theta = \theta(U) - \theta_0$, while recalling that $F'_{cap}(\theta_0) = 0$, we obtain

$$F''_{cap}(\theta_0)\delta\theta - \frac{1}{2}U^2\left[C'_{tot}(\theta_0) + C''_{tot}(\theta_0)\delta\theta\right] \simeq 0 \quad (9)$$

dx.doi.org/10.1021/la2004326 |*Langmuir* 2011, 27, 6031–6041

yielding

$$\delta\theta \simeq \frac{1}{2}\frac{C'_{tot}(\theta_0)}{F''_{cap}(\theta_0) - \frac{1}{2}U^2 C''_{tot}(\theta_0)}U^2 \quad (10)$$

and to leading order in U^2 one has

$$\theta(U) \simeq \theta_0 + \frac{1}{2}\frac{C'_{tot}(\theta_0)}{F''_{cap}(\theta_0)}U^2 \quad (11)$$

and equivalently

$$\cos\theta(U) \simeq \cos\theta_0 - \frac{1}{2}\frac{C'_{tot}(\theta_0)\sin\theta_0}{F''_{cap}(\theta_0)}U^2 \quad (12)$$

We see that, at low voltages, the deviation from the Young angle is proportional to U^2, just as in the Young−Lippmann formula. However, the prefactor is a function of θ_0 and can take different values than in eq 6, and even change its sign (see section II.D). It is shown in section IV.D under which conditions the prefactor converges to that of the Young−Lippmann formula for low voltages in typical EWOD experimental setups.

C. The High Voltage Limit. For $U \to \infty$, the electric energy becomes large relative to the capillary energy and so the minimum of F_{tot} occurs at $\theta(U) = \theta_{sat} + \delta\theta$. Expanding the condition $F'_{tot}(\theta) = 0$ around θ_{sat}, one has

$$F'_{cap}(\theta_{sat}) + F''_{cap}(\theta_{sat})\,\delta\theta - \frac{1}{2}C''_{tot}(\theta_{sat})U^2\,\delta\theta \simeq 0 \quad (13)$$

or

$$\theta(U) \simeq \theta_{sat} + \frac{F'_{cap}(\theta_{sat})}{\frac{1}{2}U^2 C''_{tot}(\theta_{sat}) - F''_{cap}(\theta_{sat})} \simeq \theta_{sat} + 2\frac{F'_{cap}(\theta_{sat})}{C''_{tot}(\theta_{sat})}U^{-2} \quad (14)$$

Hence, saturation in θ is approached asymptotically, as U^{-2}, in qualitative agreement with experiments.[12,14]

D. Reversed Electrowetting. An interesting conclusion can be drawn from the discussion in section II.A. Recalling that in our model electrowetting results from an interplay between capillary and electric energies (each with its own minimum at θ_0 and θ_{sat}, respectively); as voltage is increased, the electric energy gradually becomes dominant and the contact angle is driven away from θ_0 toward θ_{sat} (Figure 4). Since θ_0 is determined only by the capillary parameters (as in the Young formula, eq 1) and θ_{sat} is determined solely by the electric parameters, it is possible to envisage a system in which the saturation angle θ_{sat} is actually *larger* than the Young angle, $\theta_{sat} > \theta_0$ rather than $\theta_{sat} < \theta_0$ as in the usual case. In such a setup, applying a voltage will cause *an increase* of the contact angle, in total contradiction with the Young−Lippmann formula, eq 6. Hence, the model proposed here allows for the possible existence of a new regime of electrowetting, which we refer to as *reversed electrowetting*.

By examining the slopes of each energy term near the minimum of the other (see Figure 2), it is possible to show that, in the low- and high-voltage limits, eqs 11 and 14, the prefactors of both U^2 and U^{-2} terms can take either positive or negative values depending on whether $\theta_0 > \theta_{sat}$ or $\theta_0 < \theta_{sat}$; for the low-voltage limit, $F''_{cap}(\theta_0)$ is positive by definition, but $C'_{tot}(\theta_0)$ is positive only if $\theta_0 > \theta_{sat}$ and negative for $\theta_0 < \theta_{sat}$. Likewise, for the high-voltage limit, $C''_{tot}(\theta_{sat})$ is negative by definition, but $F'_{cap}(\theta_{sat})$ is negative only if $\theta_0 > \theta_{sat}$ and positive for $\theta_0 < \theta_{sat}$.

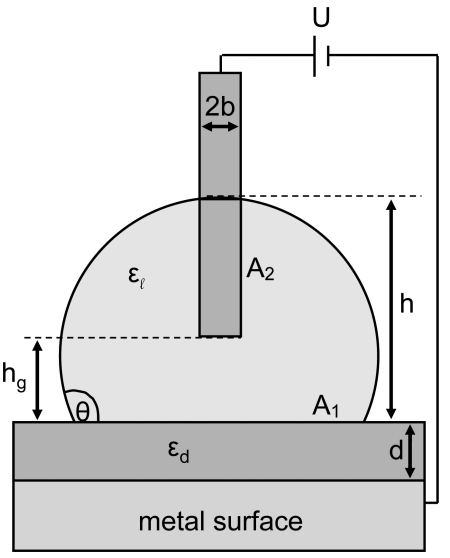

Figure 5. Schematic EWOD setup as used in our analysis. A liquid drop shaped as a spherical cap of volume V, height h, and dielectric constant ε_l is placed atop a flat metal electrode. The metal electrode is covered with a dielectric coating of thickness d and dielectric constant ε_d. A metal wire (used as a counter-electrode), modeled as a thin cylinder of radius b, is inserted into the drop from above. The gap between the two electrodes is h_g. The area of the substrate electrode covered by the drop is A_1 and that of the counter-electrode is A_2. The applied voltage is U and the contact angle with the substrate is θ.

Thus, we have shown how reversed electrowetting manifests itself in those limits.

III. A TWO ELECTRODE MODEL OF EWOD

Our goal in the remainder of this work is to elaborate on the physical conditions that are involved in determining a finite θ_{sat} angle in *specific* EWOD experimental setups. However, we would like to stress that the proposed mechanism is general and may be applied to other realizations and experimental setups manifesting CAS.

A. System Setup and Geometry. A setup of an EWOD is presented in Figure 5. The drop (dielectric constant ε_l) is assumed to retain its spherical-cap shape, with height h from the surface, total volume V, and contact angle θ. The metal electrode is coated with a dielectric layer of thickness d and dielectric constant ε_d. The top counter-electrode is modeled as a thin cylinder of radius b and the gap between the two electrodes is h_g. The two electrode areas covered by the liquid are A_1 and A_2, respectively. For spherical-cap shaped drops, A_1 and A_2 are related to the contact angle θ through the fixed volume constraint:

$$\begin{aligned} A_1 &= \pi a^2 \\ A_2 &= 2\pi b(h - h_g) \\ \tan\frac{\theta}{2} &= \frac{h}{a} \\ V &= \frac{\pi h}{6}(3a^2 + h^2) \end{aligned} \quad (15)$$

where a is the radius of the covered portion of the substrate electrode.

dx.doi.org/10.1021/la2004326 |*Langmuir* 2011, 27, 6031–6041

It should be noted that θ can only take values in the range $\theta_{min} < \theta < \pi$. The lower limit, θ_{min}, occurs when the drop height matches the gap between the lower tip of the counter-electrode and the substrate, $h = h_g$ (see Figure 5), resulting in

$$\cot\frac{\theta_{min}}{2} = \sqrt{\frac{2V}{\pi {h_g}^3} - \frac{1}{3}} \tag{16}$$

We will show that $\theta_{sat} > \theta_{min}$ and hence θ_{min} is an inaccessible lower bound of the contact angle. The upper limit $\theta = \pi$ is the dewetting limit.

B. The AC Free-Energy. The free energy, eq 8, depends on the total capacitance C_{tot}, which includes all relevant contributions. Unlike the traditional Young−Lippmann treatment in which only the capacitance of the liquid/substrate interface is taken into account, we consider explicitly the existence of an additional double-layer, residing at the interface between the liquid drop and the counter-electrode.

Experimental setups and applications usually employ AC circuits to produce an electrowetting effect. Under those circumstances, double layers are transient: with each AC half-cycle, a double layer of opposite polarity is formed at each electrode/liquid interface and subsequently dissolved away. In addition to relaxation by reversal of polarity, other mechanisms of relaxation can act at the counter-electrode/liquid interface such as electrochemical Faradic processes. The dynamical processes are, therefore, governed by two intrinsic time scales (beside the AC frequency):

1. The double-layer *build-up time*, τ_b, which can be estimated to be

$$\tau_b \simeq \frac{\lambda_D L}{D} \tag{17}$$

where $\lambda_D = [(\varepsilon_0\varepsilon_l k_B T)/(2e^2 c_{salt})]^{1/2}$ is the Debye length, $k_B T$ is the thermal energy, c_{salt} is the salt concentration, D is the diffusion constant, and L is a typical system size.[39]

2. The double-layer *relaxation time*, τ_r, which can similarly be expressed in terms of system parameters through the RC circuit relaxation formula

$$\tau_r = R_2 C_2 = \tau\frac{C_2}{A_2} \tag{18}$$

where $\rho = R_2 A_2$ is defined as the zero-current (Faradic) resistivity to charge transfer by electrochemical processes and A is the contact area.

In order to discuss the period-averaged properties of the system, we employ a standard AC circuit analysis. As shown in Figure 3b, we model the two liquid/electrode interfaces as two capacitors with capacitances C_1,C_2, defined in a similar fashion as in eq 5:

$$\begin{aligned} C_1 &= C_{ld} \simeq \frac{\varepsilon_0\varepsilon_d A_1}{d} \\ C_2 &\simeq \frac{\varepsilon_0\varepsilon_l A_2}{\lambda_D} \end{aligned} \tag{19}$$

Note that the main contribution to C_1 comes from the coated dielectric layer of thickness d ($d/\varepsilon_l \gg \lambda_D/\varepsilon_l$), while for C_2 the only contribution comes from the double layer of thickness λ_D (because the counter-electrode is *not* coated). The cylindrical geometry of the counter-electrode is not considered because $b \gg \lambda_D$.

The two capacitors are charged and discharged through a resistor R_1 that represents the bulk of the liquid drop. The relaxation of the double layer at the counter-electrode is modeled by an extra discharge circuit with a resistor R_2, while the capacitor C_1 does not have a discharge circuit since charge transfer at the substrate electrode is prevented by its dielectric coating. The appropriate resistance values can be inferred from the build-up (τ_b) and relaxation (τ_r) times, eqs 17 and 18, again through the RC circuit relaxation formula:

$$\begin{aligned} R_1 &= \tau_b\left({C_1}^{-1} + {C_2}^{-1}\right) \\ R_2 &= \frac{\tau_r}{C_2} \end{aligned} \tag{20}$$

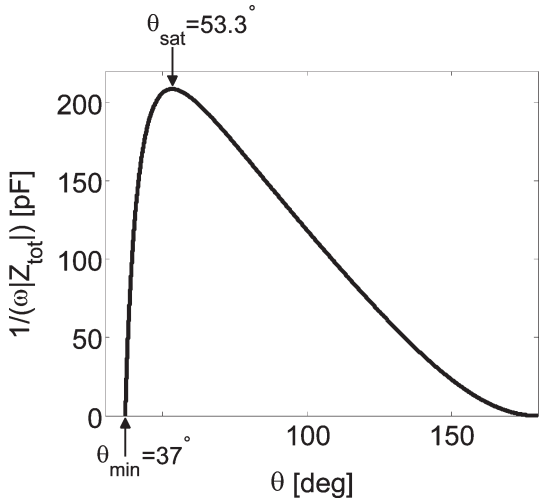

Figure 6. Total reactance $1/(\omega Z_{tot})$ (in nanoFarad) as a function of the contact angle. Parameters for the EWOD system are τ_b = 1.34 ms, τ_r = 0.53 s, and $f = \omega/2\pi$ = 1 kHz, and all other parameters are chosen as shown in Table 1. The reactance has a maximum for a finite value of θ_{sat} = 53.3°, at which the system exhibits CAS. The minimal contact angle is θ_{min} = 37°, eq 16.

Drawing on the AC circuit analogy, the period-averaged free energy is:

$$\begin{aligned} F_{tot}(\theta, U, \omega) &= F_{cap} + F_{el} \\ &= F_{cap}(\theta) - \frac{1}{2}\frac{1}{\omega|Z_{tot}(\theta,\omega)|}U^2 \end{aligned} \tag{21}$$

where U is understood to be the rms value and Z_{tot} is the total impedance of the circuit (Figure 3b), which can be represented schematically as

$$Z_{tot} = Z_{C_1} \oplus Z_{R_1} \oplus \left(Z_{C_2} || Z_{R_2}\right) \tag{22}$$

It is straightforward to show that the squared magnitude of the total impedance is

$$\begin{aligned} |Z_{tot}|^2 = &\frac{1}{{C_1}^2}\left({\tau_b}^2 + \omega^{-2}\right) + \frac{2}{C_1 C_2}\left({\tau_b}^2 + \frac{\tau_r(\tau_r + \tau_b)}{1+\omega^2{\tau_r}^2}\right) \\ &+ \frac{1}{{C_2}^2}\left({\tau_b}^2 + \frac{\tau_r(\tau_r + 2\tau_b)}{1+\omega^2{\tau_r}^2}\right) \end{aligned} \tag{23}$$

Since C_1 is proportional to A_1, which vanishes at $\theta \to \pi$, and C_2 is proportional to A_2, which vanishes at $\theta \to \theta_{min}$, $|Z_{tot}|^2$ diverges at both $\theta \to \theta_{min}$ and $\theta \to \pi$. Therefore, it must have a minimum at some intermediate value: $\theta_{min} < \theta_{sat} < \pi$. Hence, our model of

dx.doi.org/10.1021/la2004326 |*Langmuir* 2011, 27, 6031–6041

Table 1. Parameter Values of a Typical Electrowetting Setup[a]

parameter	symbol	value
dielectric constant of liquid	ε_l	80
Debye length in liquid	λ_D	1.34 nm
volume	V	5 μL
width of dielectric layer	d	0.1 μm
dielectric constant of dielectric layer	ε_d	2.67
liquid/air surface tension	γ_{la}	72.8 mN/m
dielectric/air surface tension	γ_{sa}	12.7 mN/m
liquid/dielectric interfacial tension	γ_{sl}	47 mN/m
gap between counter-electrode and substrate	h_g	0.7 mm
radius of counter-electrode	b	12.5 μm

[a] The liquid drop contains an aqueous ionic solution and is placed on top of a Miyaline-C/Teflon substrate.

Table 2. Parameter Values of a Hypothetical Reversed Electrowetting Setup

parameter	value
ε_l	2
λ_D	1.34 nm
V	5 μL
d	0.1 μm
ε_d	2.67
γ_{la}	20 mN/m
γ_{sa}	15 mN/m
γ_{sl}	5 mN/m
h_g	0.7 mm
b	12.5 μm

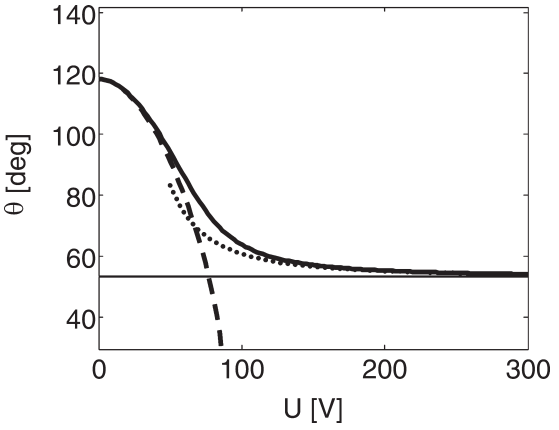

Figure 7. Calculated contact angle as a function of applied voltage, U (full line), as well as a plot of the Young–Lippmann formula (dash-dotted) using g^{eff} (dashed line, see text). Parameter values of the EWOD system are taken from Table 1 and τ_b = 1.34 ms, τ_r = 0.53 s, and $f = \omega/2\pi$ = 1 kHz. Many of the features of CAS, shown schematically in Figure 1, are reproduced. At U = 0, the contact angle is θ_0 = 118°. For small U, there is an initial compliance with the rescaled Young–Lippmann formula, eq 6, $\theta(U) \approx \theta_{YL}(U)$, followed by a crossover occurring at U^* = 76.9 V, calculated from eq 7. At larger U, the contact angle tends asymptotically to a saturation angle θ_{sat} = 53.3°. The asymptotic $\theta(U) - \theta_{sat} \sim U^{-2}$ is plotted (dotted line) following eq 14 and approximates rather well $\theta(U)$ for voltages larger than 120 V. An operational definition of the saturation voltage U_{sat} (see text) yields $U_{sat} \simeq$ 252.1 V. Note that θ_{sat} is conceivably larger than the minimal possible angle θ_{min} = 37°, eq 16.

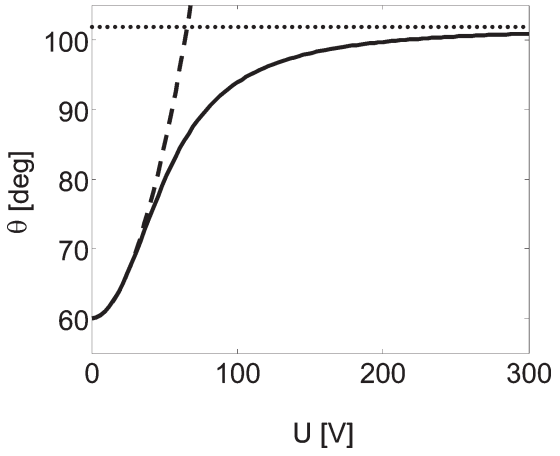

Figure 8. Calculated contact angle as a function of applied voltage, U (solid line), for reversed electrowetting together with a manually scaled ($g^{eff} < 0$) Young–Lippmann formula (dashed line). Parameter values of an EWOD system are taken from Table 2, and τ_b = 1.34 ms, τ_r = 13.2 ms, and $f = \omega/2\pi$ = 1 kHz. At U = 0, the contact angle is θ_0 = 60°. Even for small U, there is a deviation from the naive Young–Lippmann formula, eq 6, because $\theta(U) - \theta_0 \sim U^2$, with a positive prefactor. The U^2 rise is followed by a crossover occurring at U^* = 65.5 V. At larger U, the contact angle tends asymptotically to a saturation angle θ_{sat} = 101.9°. Using the same definition of the saturation voltage U_{sat} as in Figure 7 yields $U_{sat} \simeq$ 208.5 V.

electrowetting presented in section II.A is indeed applicable to typical EWOD setups.

Substituting eqs 15 and 19 into eqs 21 and 23 yields an expression for $C_1(\theta)$ and $C_2(\theta)$ and, consequently, for F_{el} as a function of θ. Its minimization can be done numerically (section IV.A) and yields the equilibrium contact angle (for given applied voltage and frequency). In some limits (sections IV.C and IV.E), analytical approximations can be derived as well.

IV. RESULTS AND DISCUSSION

A. The Electrowetting Curve, $\theta(U)$. In order to demonstrate quantitatively the model validity, we performed numerical calculations for parameter values that are in accord with some typical experimental setups. In Figure 6, we present the reactance $1/\omega Z$ (appearing in eq 21) computed for parameter values as in Table 1 and with an AC frequency $f = \omega/2\pi$ = 1 kHz. The build-up time was calculated using eq 17 to be τ_b = 1.34 ms, while the relaxation time was calculated using eq 18 with[40] $\rho = 1\ \Omega\cdot m^2$, yielding[44] τ_r = 0.53 s. For the chosen values of parameters, the ratio of capacitances for zero voltages ($\theta(U=0) = \theta_0$) is about $C_2/C_1 \simeq 25$. In the figure, a maximum at a finite angle θ_{sat} = 53.3° is clearly seen. Notably, this saturation angle is much larger than the minimal possible angle in this setup, θ_{min} = 37° (see eq 16). As a consequence, CAS is obtained for finite values of A_2, much before the limit $A_2 \to 0$ characteristic to θ_{min}.

Figure 7 presents the calculated electrowetting curve $\theta(U)$ for the same system, where $\theta(U)$ is calculated by minimizing F_{tot} from eq 21, together with a plot of the Young–Lippmann formula where an effective g^{eff} prefactor is used to fit the full calculation. This is similar to what is done in many experimental works where

dx.doi.org/10.1021/la2004326 |Langmuir 2011, 27, 6031–6041

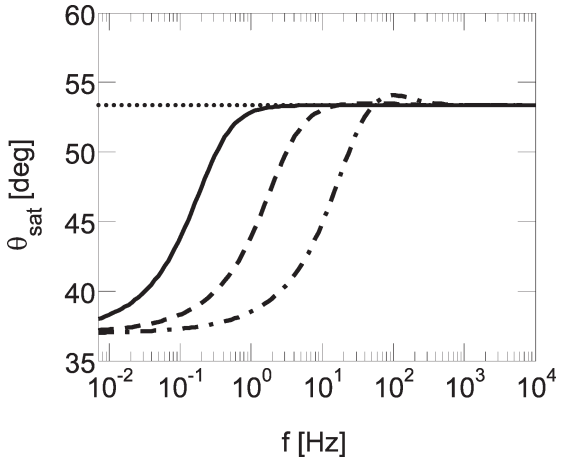

Figure 9. Saturation angle, θ_{sat}, as a function of the AC frequency f, for the EWOD system with parameter values as in Table 1, $\tau_b = 1.34$ ms, and for several τ_r values: $\tau_r = 0.53$ s (solid line), 0.053 s (dashed line), 5.3 ms (dash-dotted line). In the range $f \geq 1$ kHz, the AC saturation angle, which takes into account relaxation of the double layer by electrochemical processes, matches the $\tau_r \to \infty$ (dotted line) of $\theta_{sat}^{\infty} = 53.3°$ even for the smallest $\tau_r = 5.3$ ms (fastest Faradic relaxation).

the g value is fitted from the low U dependence, and not by using explicitly eq 6. We use a specific $g^{eff} = (1 + \omega^2\tau_b^2)^{-1/2}$ as derived in section IV.D. The figure shows that several common experimental features are reproduced (as compared with the schematic in Figure 1); an initial compliance with the scaled Young–Lippmann formula at low voltages is followed by a crossover at intermediate voltages to a different regime. Using eq 7 (with g^{eff}), the crossover voltage is evaluated to be $U^* \simeq 76.9$ V. At $U > U^*$ an asymptotic convergence of the contact angle toward a saturation value is seen, $\theta(U) \to \theta_{sat} = 53.3°$. This is further demonstrated in Figure 7, where the asymptotic $\theta(U) - \theta_{sat} \sim U^{-2}$ is plotted (dotted line) following eq 14. The asymptotic behavior approximates rather well $\theta(U)$ for voltages larger than 120 V.

It is appropriate to define another voltage, U_{sat}, characterizing the saturation range of the potential. An operational definition that we employ is that at U_{sat}, the calculated $\theta(U_{sat})$ deviates from θ_{sat} by 2%. With this definition, we obtain $U_{sat} \simeq 252.1$ V. The electrowetting curve presented in Figure 7 agrees qualitatively with experimental observations,[8,12,28] which show the effect of contact angle saturation. Unfortunately, because the parameter values needed for quantitative comparison with experiments are lacking at present, we used instead reasonable estimations.

B. The Reversed Electrowetting Curve, $\theta(U)$. We now illustrate how reversed electrowetting $\theta_{sat} < \theta_0$, which is a natural outcome of our model, can be seen in the laboratory. Let us consider a system similar to the one presented in the previous section with the two following changes (see Table 2): the interfacial tensions are chosen such that $\theta_0 = 60°$, and we now model a nonpolar liquid with a dielectric constant $\varepsilon_l = 2$, which yields a build-up time of $\tau_b = 1.34$ ms and a relaxation time of $\tau_r = 13.2$ ms. The AC frequency is $f = \omega/2\pi = 1$ kHz as before.

Figure 8 presents the calculated electrowetting curve $\theta(U)$. The plot features an initial compliance with the negatively rescaled Young–Lippmann formula (at low voltages such that the contact angle *increases* with the applied voltage). This is followed by a crossover at intermediate voltages toward saturation. Using eq 7 (with g^{eff}), the crossover voltage is evaluated to be $U^* \simeq 65.5$ V. For $U > U^*$, an asymptotic convergence of the contact angle toward a saturation value is seen, $\theta(U) \to \theta_{sat} = 101.9°$. Using the same definition as in section IV.A, the saturation voltage is found to be $U_{sat} \simeq 208.5$ V.

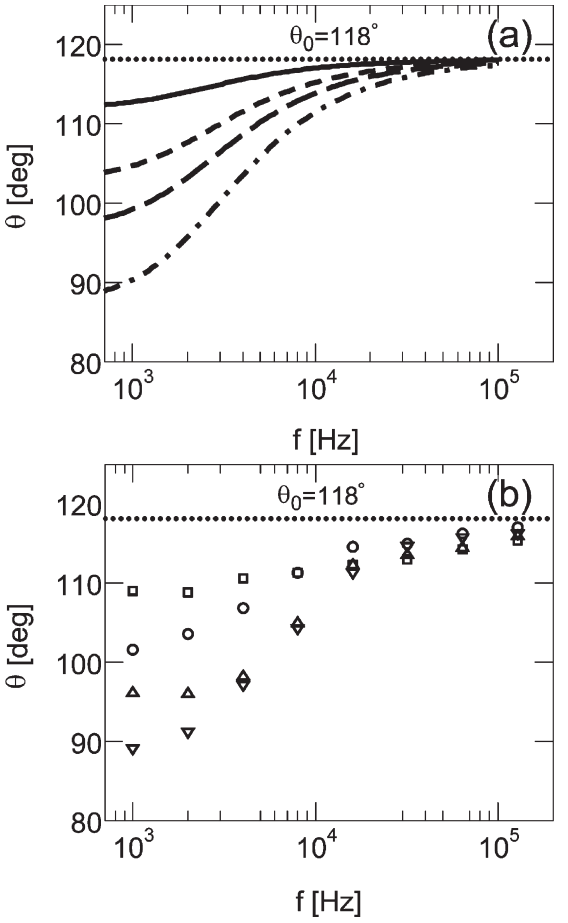

Figure 10. Contact angle as function of AC frequency f for several applied voltages U. (a) Calculated values corresponding to 57 V (solid line), 93 V (short dashed line), 113 V (long dashed line), and 143 V (dash-dotted line) with parameters as in Table 3 and $\tau_b = 0.1$ ms, $\tau_r = 2.4$ ms. The value of $\theta_0 = 118°$ is indicated by a dotted line. (b) Experimental results adapted from ref 8 for the same voltages as in (a): (□) 57 V, (○) 93 V, (△) 113 V, and (▽) 143 V. A quantitative agreement between the calculation and experiment can be seen. Note also that the electrowetting effect diminishes at high frequencies as predicted analytically in eq 24.

Since our reversed electrowetting predictions (Figure 7) are rather for specific parameter values, it will be of benefit to check their validity with experiments conducted on similar electrowetting setups.

C. The Frequency Dependence of Electrowetting. In order to explore the effect of the frequency of the AC voltage within our model, the dependence of the saturation angle θ_{sat} on frequency was calculated numerically by minimizing eq 21 and plotted in Figure 9 for several values of $\tau_r = 0.53$ s, 0.053 s, and 5.3 ms. It can be seen that, for this specific choice of parameters, the AC saturation angle reaches a constant value for the entire high frequency range down to $f \simeq 1$ kHz, even for the smallest of the chosen relaxation times ($\tau_r = 5.3$ ms). Moreover, the larger τ_r is, the wider is the range for which the saturation angle is constant. This can be explained by taking into account that

dx.doi.org/10.1021/la2004326 |*Langmuir* 2011, 27, 6031–6041

Table 3. Parameter Values of an Electrowetting System of Deionized Water Solution on Miyaline-C/Teflon Substrate[a]

parameter	value
ε_l	80
λ_D	300 nm (fitted)
V	5 μL
d	5 μm
ε_d	2.67
γ_{la}	72.8 mN/m
γ_{sa}	12.7 mN/m
γ_{sl}	47 mN/m
h_g	0.7 mm
b	40 μm

[a] The parameter values are inferred from ref 8, except for λ_D, which was fitted to obtain a quantitative agreement with experiments. The resulting value is indeed compatible with that of deionized water (ionic strength less than 10^{-6} M).[45]

whenever $\tau_r \gg 1/f$, the counter-electrode double layer can hardly relax.

The frequency dependence of the contact angle has been experimentally studied in ref 8 for several applied voltages. Figure 10 shows a comparison of a minimization of eq 23 for a range of frequencies, with experimental data. The calculations have been performed for system parameters as in Table 3, which have been inferred[45] from ref 8, except for λ_D = 300 nm, which was used as a fitting parameter to the experimental results. This value corresponds to ionic strength of less than 10^{-6} M and is compatible with deionized water used in ref 8. The build-up time was deduced from the featured experimental results to be τ_b = 0.1 ms, and the relaxation time, τ_r = 2.4 ms, was calculated using eq 18 with $\rho = 1\ \Omega\cdot m^2$.

Comparison of the two plots shows that our model reproduces rather well the frequency dependence found in experiments. It can be seen that the electrowetting effect diminishes with rising frequency and seems to vanish at f > 100 kHz where there is hardly any deviation from the Young angle. This can be easily understood taking into account that for f > 10 kHz, $1/f$ becomes small as compared to the double layer build-up time $\tau_b \simeq 0.1$ ms. Under those circumstances, ions move too slowly and cannot build considerable over-concentrations at the electrodes. Thus, at those high frequencies, the period-averaged effect of the double layers decreases considerably.

The above results imply that it is of value to further explore the limit of slow electrochemical processes, $\tau_r \gg \tau_b$, $\omega\tau_r \gg 1$, which leads to a simplified expression for the free energy. Substituting eq 23 into eq 21 we obtain in this limit

$$|Z_{tot}| \approx \frac{\sqrt{\tau_b^2 + \omega^{-2}}}{C_{tot}(\theta)}$$

$$F_{el}(\theta, U, \omega) = -\frac{1}{2\omega|Z_{tot}|}U^2 \approx -\frac{C_{tot}(\theta)}{2\sqrt{1+\omega^2\tau_b^2}}U^2 \quad (24)$$

where $C_{tot}^{-1} = C_1^{-1} + C_2^{-1}$ is the total capacitance of an equivalent system without any electrochemical processes. The $(1+\omega^2\tau_b^2)^{-1/2}$ prefactor in eq 24 depends on the AC frequency and reflects a diminishing electrowetting effect for rising frequencies.

We note that the DC limit can be obtained by first assuming no electrochemical processes, $\tau_r \to \infty$ in eq 23 (leading to eq 24), and only then taking the DC limit of $\omega \to 0$ to get $F_{el} = -{}^1/_2 C_{tot} U^2$ of eq 8. This limit can be useful in applications where both the substrate and counter-electrode are dielectrically coated.

If electrochemical processes are not totally excluded but are just slow (order of seconds, in accordance with the value calculated in section IV.A), it is expected that the results obtained in this work will be applicable for that time scale, above which other mechanisms might take over. Such time-dependent behavior has been observed in ref 24.

D. Convergence to the Young−Lippmann Formula. In its DC limit ($\omega \to 0$), eq 24 provides a pathway to establish a relationship between our model and the Young−Lippmann formula and to show the conditions under which the two converge. Using eqs 15 and 19 (see Appendix for more details), we have

$$C_{tot} = C_1\left[1+\frac{C_1}{C_2}\right]^{-1} = C_1\left[1+\beta^{-1}\frac{2-\xi^3}{\xi^2 - l^{-1}h_g\xi}\right]^{-1} \quad (25)$$

where $l \equiv (3V/\pi)^{1/3}$ is a typical drop length,

$$\beta \equiv \frac{6\varepsilon_l db}{\varepsilon_d \lambda_D l} \quad (26)$$

is a dimensionless parameter, and

$$\xi \equiv \left[\frac{1-\cos\theta}{2+\cos\theta}\right]^{1/3} \quad (27)$$

is a monotonically increasing function of $0 \le \theta \le \pi$.

As long as the second term in the brackets of eq 25 is small, our model agrees with the standard model, $F_{el} = -{}^1/_2 C_1 U^2$, eq 4, with $C_1 = C_{ld}$. For a typical system, as the one presented in Table 1, the value of the constant prefactor is rather small $\beta^{-1} \simeq 0.01$. Since $h_g/l \le \xi \le 2^{1/3}$, it is clear that the quotient can only be large when $\xi \to h_g/l$ or, equivalently, when the contact angle becomes small enough. Otherwise, the second term is negligible and the two models converge.

Note that this view of the validity of the Young−Lippmann formula as being related to a certain *range of the contact angles* is a departure from the common approach which regards its validity being related to a certain *range of applied voltages*.

By creating this link between the Young−Lippmann formula and our model it can be deduced that the proper way of extending the Young−Lippmann formula (within its validity range) from DC to AC is to replace $U^2 \to U_{rms}^2/(1+\omega^2\tau_b^2)^{1/2}$. This is exactly the how the Young−Lippmann formula was scaled (by $g^{(eff)}$) in section IV.A.

E. The Saturation Angle for Slow Relaxation ($\omega\tau_r \gg 1$, $\tau_r \gg \tau_b$). Within the slow relaxation framework, eq 24, the minimization of F_{el} (yielding θ_{sat}) is equivalent to minimizing the total inverse capacitance $\alpha \equiv 1/C_{tot}$. Using eqs 15 and 19, we obtain

$$\alpha(\xi) = \frac{3d}{2\pi\varepsilon_0\varepsilon_d l^2}\left[\frac{1}{\xi^{-1} - \frac{1}{2}\xi^2} + \frac{2\beta^{-1}}{\xi - l^{-1}h_g}\right] \quad (28)$$

dx.doi.org/10.1021/la2004326 |*Langmuir* 2011, 27, 6031–6041

Minimizing $\alpha(\xi)$ yields a sixth-order polynomial in ξ:

$$\xi^6 - 2\beta\xi^5 + 4\beta l^{-1}h_g\xi^4 - 2\left(2 + \beta l^{-2}h_g{}^2\right)\xi^3 - 2\beta\xi^2 + 4\beta l^{-1}h_g\xi + 2\left(2 - \beta l^{-2}h_g{}^2\right) = 0 \quad (29)$$

It is possible to examine two separate limits for minimizing $\alpha(\xi)$, leading to two simple analytical expressions for θ_{sat}.

1. Acute Saturation Angles (Large β). If $\xi^3(\theta_{sat}) \ll 2$, then, near its minimum, eq 28 reduces to

$$\alpha\big|_{\xi \simeq \xi_{sat}} \simeq \frac{3d}{2\pi\varepsilon_0\varepsilon_d l^2}\left[\xi + \frac{2\beta^{-1}}{\xi - l^{-1}h_g}\right] \quad (30)$$

with a minimum at $\xi = \xi_{sat}$ that satisfies

$$1 - 2\beta^{-1}\left(\xi_{sat} - \frac{h_g}{l}\right)^{-2} = 0 \quad (31)$$

The solution yields

$$\xi_{sat} = \sqrt{\frac{2}{\beta}} + \frac{h_g}{l} \quad (32)$$

and θ_{sat} can now be obtained

$$\cos\theta_{sat} = \frac{1 - 2\xi_{sat}^3}{1 + \xi_{sat}^3} \quad (33)$$

Inserting typical values from Table 1 to check for self-consistency, we get $\xi_{sat}^3 \approx 0.173 \ll 2$ as required. Using eq 33, the saturation angle in this case is calculated to be $\theta_{sat} \simeq 56.1°$, which is not far from the value obtained by a full numerical calculation, 53.3°. As a rule of thumb, we remark that the above condition, $\xi_{sat}^3 \ll 2$ holds for θ_{sat} smaller than $\pi/2$, for which $\xi^3(\pi/2) = 0.5 \ll 2$.

2. Large Saturation Angles (Small β and h_g/l). For systems with small β, the above approximation should fail, as is apparent from eq 32. For such cases, we can use a different approximation assuming that the gap h_g is small enough, such that

$$\xi_{sat} \gg \frac{h_g}{l} \quad (34)$$

The saturation angle can then be found from a different approximated form of $\alpha(\xi)$ (eq 28), near its minimum:

$$\alpha\big|_{\xi \simeq \xi_{sat}} \simeq \frac{3d}{2\pi\varepsilon_0\varepsilon_d l^2}\left[\frac{1}{\xi^{-1} - \frac{1}{2}\xi^2} + \frac{2\beta^{-1}}{\xi}\right] = \frac{3d}{\pi\varepsilon_0\varepsilon_d l^2}\left[\frac{1}{2 - \xi^3} + \beta^{-1}\right]\xi^{-1} \quad (35)$$

Minimizing $\alpha(\xi)$, we get a quadratic equation in the variable ξ^3:

$$\xi^6 - 4(\beta + 1)\xi^3 + 2(\beta + 2) = 0 \quad (36)$$

whose solution is

$$\xi_{sat}^3 = 2(\beta + 1) \pm \sqrt{4(\beta + 1)^2 - 2(\beta + 2)} \quad (37)$$

For small β, it is possible to further simplify the expression for ξ_{sat} to obtain

$$\xi_{sat}^3 \simeq 2\left(1 - \sqrt{\frac{3\beta}{2}}\right) \quad (38)$$

Checking for self-consistency, the condition holds for small enough gaps.

V. SUMMARY AND OUTLOOK

In this work, we propose a novel approach toward electrowetting that, among other results, can account for contact angle saturation (CAS) applicable to some electrowetting setups. The model is based on a generalized version of the free energy accounting for various electric contributions. The interplay between the capillary (F_{cap}) and electric (F_{el}) terms depends on the applied voltage U, because $F_{el} \sim -U^2$. Therefore, when an external voltage is applied, it will drive the system away from its capillary free energy minimum and toward its electric free energy minimum.

Our approach is distinctly different from other views of electrowetting that make use of the Young−Lippmann formula. In our model, the electric term can exhibit a variety of dependencies on the contact angle as determined by the exact system geometry. Particularly, if the electric term F_{el} has a global minimum at a certain contact angle θ_{sat}, then for high enough voltages this angle also minimizes (asymptotically) the *total* free energy F_{tot}. Additional increase of the applied voltage does not change the location of the global minimum, and the contact angle saturates at θ_{sat}. We identify exactly this angle with the saturation angle found in experiments. This very general assumption (F_{el} with a minimum) is all that is needed to show that in the low-voltage limit a Young−Lippmann compatible $\sim U^2$ behavior is expected, while in the high-voltage limit an $\sim U^{-2}$ saturation should be present. Numerical calculations suggest that combination of these two limiting behaviors approximates rather well the full expression for $\theta(U)$ in the whole voltage range.

When applying our approach to EWOD setups, we take two contributions to F_{el} into account: (i) the double layer at the drop/substrate interface and (ii) another double layer at the drop/counter-electrode interface. The latter was previously unaccounted for because it was considered to be negligible due to geometry, or that its relaxation time was considered to be very fast. However, we estimate the relaxation time to be long (on the order of seconds) and, therefore, the effect of the counter-electrode double-layer cannot be neglected for AC systems. Similarly, it cannot be neglected for low voltages (which will exclude electrochemical processes from taking place at all)[27] or in DC applications that include a dielectrically coated counter-electrode. Using AC circuit analysis, we show that F_{el} indeed has a global minimum that produces the CAS effect.

The value of the saturation angle as well as the entire electrowetting curve $\theta(U)$ can be found numerically for any choice of system parameters, and our specific choice is inspired by the experiments reviewed in ref 12. There is a qualitative agreement with experimental results, which includes an initial compliance with the Young−Lippmann formula (scaled correctly), followed by a crossover to CAS. The values obtained for the saturation angle, crossover voltage, and saturation voltage are also compatible with experimental values.

In addition, we investigated the frequency dependence of electrowetting. It is shown that the value of the saturation angle is independent of the AC frequency for a large range of frequencies (1−100 kHz) for a specific choice of parameters. A numerical analysis of the frequency dependence of electrowetting was conducted for a set of system parameters inferred from ref 8 and shows semiquantitative agreement with the experiment. These results show that an approximation of the free energy

dx.doi.org/10.1021/la2004326 |*Langmuir* 2011, 27, 6031–6041

can be justified, such that the entire frequency dependence is captured in a scaling factor of the applied voltage. It predicts that the electrowetting effect should diminish with rising frequency, as indeed found in experiments.[8]

In its DC limit, our model can converge to the Young−Lippmann formula, depending on the values of the Young and saturation angles. We use this result to show a novel way to extend the Young−Lippmann formula from DC to AC systems. We conclude that the validity of the Young−Lippmann formula is related not to the range of applied voltages, as it is commonly viewed, but rather to the accessed range of contact angles. In commonly used EWOD setups, which are intentionally devised to have as high a Young angle and as low a saturation angle as possible (so the effect can be more easily measured), our model is compatible with a compliance to the Young−Lippmann formula at low voltages (and hence high contact angles). We note that the DC limit of our model can be most useful in DC applications that employ low voltages and/or include a dielectrically coated counter-electrode.

Our model does not rely on any leakage mechanisms to predict CAS. Nevertheless, we would like to stress that leakage mechanisms treated in previous works[7,22,26,31−33] can be added. Interestingly, it is conceivable that a crossover between inherent CAS (as in the present model) and CAS originating from leakage mechanisms is responsible for the time-dependent saturation angle reported in ref 24.

The fact that the saturation angle depends on electric parameters whereas the Young angle depends on the capillary parameters leads to the surprising possibility of *reversed electrowetting*. Therefore, it may be possible to construct a system in which the Young angle is *lower* than the saturation angle. In such a system, the effect of applying an external voltage would be an *increase* in the contact angle, in total contradiction with the Young−Lippmann formula that allows only a decrease in the contact angle. We give an example of a choice of parameters that should yield reversed electrowetting.

Recently, the separate control of the Young and saturation angles was demonstrated in experiments.[46] This ability was utilized to construct a set of dye cells[47] that are "complementary" in their opposite response to applied voltage (black-to-white or vice versa). We believe that further research in this direction will provide ample opportunity to test for the existence of reversed electrowetting. Finding such evidence would have a potential impact that can go much beyond our specific model.

We hope that some of the predictions presented in this paper will be tested in future experiments in a quantitative fashion, gaining more insight on electrowetting and the CAS phenomenon. For example, it will be interesting to study how retracting the counter-electrode and, hence, reducing its contact area A_2 affects the saturation angle, as well as coating it with a dielectric material. Our results suggest that more research into processes taking place at the counter-electrode is needed, especially with regards to CAS in DC EWOD setups.

APPENDIX

It is convenient to express the geometrical parameters and the capacitances in terms of a monotonic function of the contact angle

$$\xi(\theta) = \left(\frac{1-\cos\theta}{2+\cos\theta}\right)^{1/3} \tag{A.1}$$

where $l = (3V/\pi)^{1/2}$, derived from the drop volume V, is a characteristic length.

The geometrical parameters defined in eq 15 can then be written as

$$\begin{aligned} h &= l\xi(\theta) \\ a &= \sqrt{\frac{1}{3}}l\left(2\xi^{-1}-\xi^2\right)^{1/2} \\ A_1 &= \frac{\pi l^2}{3}\left(2\xi^{-1}-\xi^2\right) \\ A_2 &= 2\pi b h_g\left(l h_g^{-1}\xi - 1\right) \end{aligned} \tag{A.2}$$

Combining the above expressions with the definitions of the two capacitances, we obtain

$$\begin{aligned} C_1 &= \frac{\pi}{3}\frac{\varepsilon_0\varepsilon_d l^2}{d}\left(2\xi^{-1}-\xi^2\right) \\ C_2 &= 2\pi b l\frac{\varepsilon_0\varepsilon_l}{\lambda_D}\left(\xi - l^{-1}h_g\right) \end{aligned} \tag{A.3}$$

With the use of a dimensionless parameter

$$\beta = \frac{6\varepsilon_l}{\varepsilon_d}\frac{db}{\lambda_D l} \tag{A.4}$$

the ratio between the two capacitances can finally be expressed as

$$\frac{C_1}{C_2} = \beta^{-1}\frac{2-\xi^3}{\xi^2 - l^{-1}h_g\xi} \tag{A.5}$$

AUTHOR INFORMATION

Corresponding Author

*E-mail: andelman@post.tau.ac.il.

ACKNOWLEDGMENT

We thank M. Bazant, D. Ben-Yaakov, B. Berge, T. Blake, H. Diamant, T. B. Jones, M. Maillard, A. Marmur, F. Mugele, R. Shamai, A. Steckl, U. Steiner, V. Tsionsky, and Y. Tsori for many useful discussions and comments. Support from the Israel Science Foundation (ISF) under Grant Nos. 231/08 and 1109/09 and the US−Israel Binational Science Foundation (BSF) under Grant No. 2006/055 is gratefully acknowledged.

REFERENCES

(1) Rinkel, P. D.; Minnema, L.; Barneveld, H. A. *IEEE Trans. Electr. Insul.* **1980**, *15*, 461.
(2) Jackle, J. A.; Hackwood, S.; Veselka, J. J; Beni, G. *Appl. Opt.* **1983**, *22*, 1765.
(3) Gorman, C. B.; Biebuyck, H. A.; Whitesides, G. M. *Langmuir* **1995**, *11*, 2242.
(4) Sondag-Huethorst, J. A. M.; Fokkink, L. G. J. *Langmuir* **1994**, *10*, 4830.
(5) Vallet, M.; Berge, B.; Vovelle, L. *Polymer* **1996**, *37*, 2465.
(6) Welters, W. J. J.; Fokkink, L. G. J. *Langmuir* **1998**, *14*, 1535.
(7) Vallet, M.; Vallade, M.; Berge, B. *Eur. Phys. J. B* **1999**, *11*, 583.
(8) Hong, J. S.; Ko, S. H.; Kang, K. H.; Kang, I. S. *Microfluid. Nanofluid.* **2007**, *5*, 263.
(9) Monroe, C. W.; Urbakh, M.; Kornyshev, A. A. *J. Phys.: Condens. Matter* **2007**, *19*, 375113.

(10) Monroe, C. W.; Daikhin, L. I.; Urbakh, M.; Kornyshev, A. A. *J. Phys.: Condens. Matter* **2006**, *18*, 2837. Monroe, C. W.; Daikhin, L. I.; Urbakh, M.; Kornyshev, A. A. *Phys. Rev. Lett.* **2006**, *97*, 136102.
(11) Jones, T. B.; Fowler, J. D.; Chang, Y. S.; Kim, C. J. *Langmuir* **2003**, *19*, 7646.
(12) Mugele, F.; Baret, J. C. *J. Phys.: Cond. Mat.* **2005**, *17*, R705.
(13) Herberth, U. Ph.D. Thesis, Albert-Ludwigs University, Freiburg 2006 (unpublished).
(14) Shamai, R.; Andelman, D.; Berge, B.; Hayes, R. *Soft Matter* **2008**, *4*, 38.
(15) Salata, O. V. *Curr. Nanosci.* **2005**, *1*, 25.
(16) Pollack, M. G.; Fair, R. B.; Shenderov, A. D. *Appl. Phys. Lett.* **2000**, *77*, 1725.
(17) Darhuber, A. A.; Troian, S. M. *Ann. Rev. Fluid Mech.* **2005**, *37*, 425.
(18) Feenstra, J.Hayes, R.Liquivista Inc., internal communication, 2006.
(19) Berge, B.; Peseux, J. *Eur. Phys. J. E* **2000**, *3*, 159.
(20) Esinenco, D.; Codreanu, I.; Rebigan, R. *CAS 2006 Proc., Int. Semicond. Conf.* **2006**, *2*, 443.
(21) Adamiak, K. *Microfluid Nanofluid* **2006**, *2*, 471.
(22) Shapiro, B.; Moon, H.; Garrell, R. L.; Kim, C. J. *J. Appl. Phys.* **2003**, *93*, 5794.
(23) Restolho, J.; Mata, J. L.; Saramago, B. *J. Phys. Chem. C* **2009**, *113*, 9321.
(24) Quinn, A.; Sedev, R.; Ralston, J. *J. Phys. Chem. B* **2005**, *109*, 6268.
(25) Quilliet, C.; Berge, B. *Curr. Opin. Colloid Interface Sci.* **2001**, *6*, 34.
(26) Verheijen, H. J. J.; Prins, M. W. J. *Langmuir* **1999**, *19*, 6616.
(27) Berry, S.; Kedzierski, J.; Abedian, B. *J. Colloid Interface Sci.* **2006**, *303*, 517.
(28) Millefiorini, S.; Tkaczyk, A. H.; Sedev, R.; Efthimiadis, J.; Ralston, J. *J. Am. Chem. Soc.* **2006**, *128*, 3098.
(29) Jones, T. B.; Wang, K. L. *Appl. Phys. Lett.* **2005**, *86*, 054104.
(30) Jones, T. B.; Wang, K. L.; Yao, D. J. *Langmuir* **2004**, *20*, 2813.
(31) Papathanasiou, A. G.; Papaioannou, A. T.; Boudouvis, A. G. *J. Appl. Phys.* **2008**, *103*, 034901.
(32) Fontelos, M. A.; Kindelan, U. *Q. J. Mech. Appl. Math.* **2009**, *62*, 465.
(33) Papathanasiou, A. G.; Boudouvis, A. G. *Appl. Phys. Lett.* **2005**, *86*, 164102.
(34) Young, T. *Philos. Trans. R. Soc. London* **1805**, *95*, 65.
(35) Quere, D.; de Gennes, P. G.; Brochard-Wyart, F.; Reisinger, A. *Capillarity and Wetting Phenomena: Drops, Bubbles, Pearls, Waves*; Springer: New York, 2004.
(36) de Gennes, P. G. *Rev. Mod. Phys.* **1985**, *57*, 827.
(37) The contribution of the counter-electrode to the capillary energy can be neglected here based on its small dimensions.
(38) Kang, K. H. *Langmuir* **2002**, *18*, 10318–10322. Walker, S. W.; Shapiro, B. *J. Microelectromech. Syst.* **2006**, *15*, 986–1000. Schertzer, M. J.; Gubarenko, S. I.; Ben-Mrad, R.; Sullivan, P. E. *Langmuir* **2010**, *26*, 19230–19238. Cho, S. K.; Moon, H. J.; Kim, C. J. *J. Microelectromech. Syst.* **2003**, *12*, 70–79. Ren, H.; Fair, R. B.; Pollack, M. G.; Shaughnessy, E. J. *Sens. Actuators, B* **2002**, *87*, 201–206.
(39) Bazant, M. Z.; Thornton, K.; Ajdari, A. *Phys. Rev. E* **2004**, *70*, 021506.
(40) According to refs 41−43, experiments on biosensors have shown that the zero-current Faradic resistivity ρ of a number of metallic electrodes in standard saline (150 mM/L) is of the order of $\rho \simeq 0.3-1.4\ \Omega \cdot m^2$. They further reported that these values stay in the same order of magnitude for current densities up to 0.1 $\mu A/m^2$. Since leakage currents in electrowetting experiments are much smaller, on the order of 0.1 nA/m^2 (see ref 31), the chosen values of ρ can hence be justified.
(41) Mayer, S.; Geddes, L. A.; Bourland, J. D.; Ogborn, L. *Australas. Phys. Eng. Sci. Med.* **1992**, *15*, 38.
(42) Mayer, S.; Geddes, L. A.; Bourland, J. D.; Ogborn, L. *Med. Biol. Eng. Comput.* **1992**, *30*, 538.
(43) Geddes, L. A.; Roeder, R. *Ann. Biomed. Eng.* **2001**, *29*, 181.
(44) Note that this value means that the counter-electrode does not relax momentarily as is implied by the naive application of the Young−Lippmann formula to AC EWOD setups, which suggests $\tau_r \rightarrow 0$.
(45) V, γ_{la}, and d are reported in ref 8, while ε_d, ε_l, γ_{sa}, and γ_{sl} are assigned reasonable values according to the materials used there, and h_g and b are estimated from photos it provides.
(46) Kim, D. Y.; Steckl, A. J. *Langmuir* **2010**, *26*, 9474.
(47) The dye cell of ref 46 contains a drop of colored oil that is immersed in a transparent electrolyte. The two fluids compete to occupy the surface area of the substrate. Applied voltage changes the result of the competition. Such micrometer-scale dye cells can be embedded on a proper substrate to be used as electronic ink in e-paper applications.